Global Journal of Pure and Applied Mathematics.
ISSN 0973-1768 Volume 14, Number 8 (2018), pp. 1101–1119

http://www.ripublication.com/gjpam.htm

Hydromagnetic Jeffery-Hamel Unsteady Flow of a Dissipative Non-Newtonian Fluid with Nonlinear Viscosity and Skin Friction

Francis Oketch Ochieng[1]
Department of Mathematics, Pan African University,
Institute for Basic Sciences,
Technology and Innovations (PAUISTI),
P.O. Box 62000-00200, Nairobi, Kenya.

Mathew Ngugi Kinyanjui
Department of Pure and Applied Mathematics,
Jomo Kenyatta University of Agriculture and Technology (JKUAT),
P.O. Box 62000-00200, Nairobi, Kenya.

Mark Eric Kimathi
Department of Mathematics and Statistics,
Machakos University (MKsU),
P.O. Box 136-90100, Machakos, Kenya.

Abstract

In this paper, the unsteady two-dimensional Jeffery-Hamel flow of an incompressible non-Newtonian fluid, with nonlinear viscosity and skin friction, flowing through a divergent conduit in the presence of a constant applied magnetic field in the direction perpendicular to the fluid motion is studied. The resulting nonlinear partial differential equations governing this flow problem are reduced into a system of nonlinear ordinary differential equations using similarity transformation. The resulting boundary value problem is solved numerically using the collocation method and implemented in MATLAB using the bvp4c inbuilt function to obtain the numerical solution. The effect of varying Reynolds number Re, Hartmann number Ha, Prandtl number Pr, Eckert number Ec, and unsteadiness parameter λ on the fluid velocity, fluid temperature, skin-friction, and heat transfer rate are presented in form of graphs and tables; and are discussed. From the results, it is noted that there are

[1]Correspondence author: E-mail: francokech@gmail.com

significant effects of pertinent parameters on the flow variables. This study provides useful information for engineering, technological, and industrial applications such as in hydromagnetic power generators.

AMS subject classification: 26D15, 34K20, 39B82.
Keywords: Ferrofluid, Jeffery-Hamel flow, magnetohydrodynamics, non-Newtonian fluid, nonlinear viscosity, similarity transformation, skin-friction.

Nomenclature
$(r, \theta, z)-$ Cylindrical co-ordinate variables
$(u_r, u_\theta, u_z)-$ Cylindrical velocity components
$T_\infty-$ Free stream temperature (K)
T_w- Wall temperature (K)
$T-$ Temperature (K)
$t-$ Time (s)
$U_\infty-$ Free stream velocity (m/s)
$F-$ Dimensionless fluid velocity
C_p- Specific heat at constant pressure (J/kg·K)
C_f- Skin-friction coefficient
$k-$ Thermal conductivity (W/mK)
B_0- Constant magnetic field intensity ($\mathrm{Nm^{-1}A^{-1}}$)
$n-$ Flow behavior index

Greek symbols
$\sigma-$ Electrical conductivity ($\Omega^{-1}\mathrm{m}^{-1}$)
$\rho-$ Fluid density (kgm^{-3})
$\mu-$ Coefficient of dynamic viscosity (Nsm^{-2})
μ_0- Fluid consistency coefficient (Pa s^n)
$\delta-$ Time-dependent length scale (m^{-2})
$\theta-$ Wedge semi-angle
$\varpi-$ Wedge angle
$\omega-$ Dimensionless fluid temperature
$\Psi-$ Stream function
$\gamma-$ Friction coefficient factor
$\varepsilon-$ Wedge angle parameter
$\Xi-$ Flow property/variable

1. Introduction

Fluid flow through a convergent (or divergent) wedge has gained a lot of interest due to the wide range of applications in the field of engineering and technology. Mathematical

formulation of viscous fluid flow in a wedge-shaped passage was pioneered by Jeffery in 1915 and Hamel in 1916. Therefore, this type of flow is referred to as the Jeffery-Hamel flow. Thus, Jeffery-Hamel flow refers to a flow with a source or sink of fluid volume at the point of intersection of two plane walls which are either convergent or divergent.

A non-Newtonian fluid refers to a fluid whose coefficient of dynamic viscosity is a variable. In practice, many fluid materials exhibit non-Newtonian fluid behavior such as salt solutions, toothpaste, starch suspensions, paint, blood, and shampoo [11]. It is important to note here that many fluids of industrial importance are non-Newtonian. In real industrial applications, non-Newtonian fluids are more appropriate than Newtonian fluids due to their applications in petroleum drilling, polymer processing, certain separation processes, manufacturing of foods and paper, and some other industrial processes [2].

Magnetohydrodynamics (MHD) was first introduced by Alfvén in 1970. The theory of MHD involves electromagnetic induction in a moving electrically conducting fluid in the presence of an applied magnetic field. Such induction exerts a force on ions of the electrically conducting fluid. The description is as follows: if an electrically conducting fluid is placed in a constantly applied magnetic field, the motion of the fluid induces currents which create forces on the fluid. The production of these currents has led to their use in engineering and industrial applications [7]. The theoretical study of MHD flow has been a subject of great interest due to its extensive applications in engineering processes such as in MHD power generators for electricity production, accelerators, MHD pumps, MHD flow meters, electrostatic filters, the design of cooling systems with liquid metals, and in geothermal power stations [9, 15]. Considerable efforts have been done to study the MHD theory for technological application of fluid pumping system in which electrical energy forces the working of electrically conducting fluid.

Hydromagnetic Jeffery-Hamel flow has gained considerable attention due to its applications in industrial and biological sciences. Moreover, the heat and mass transfer analysis play a vital role in the handling and processing of non-Newtonian fluids. The radiation effects have important applications in Physics and engineering processes. The radiations due to heat transfer effects on different flows are very important in space technology and high-temperature processes. Thermal radiation effects may play an important role in controlling heat transfer in polymer processing industries where the quality of the final product depends on the heat and mass controlling factors. High-temperature plasma, cooling of nuclear reactors, and power generation systems are some important applications of radiation heat transfer [13]. The consideration of MHD flow in a wedge-shaped is quite significant in crystal growth, the design of medical diagnostic devices, control of liquid metal flows, etc. Furthermore, several engineering processes such as fossil fuel combustion energy, astrophysical flows, gas turbines, solar power technology and many propulsion devices for aircraft, satellites, missiles, and space vehicle occur at high temperatures and hence thermal radiation effect becomes important. In particular, thermal radiation has a central role in engineering processes occurring at high temperatures for the design of many advanced energy conversion systems and pertinent equipment [12].

In their study of the unsteady two-dimensional flow of MHD non-Newtonian Maxwell fluid over a stretching surface with a prescribed surface temperature in the presence of heat source or sink, [4] found numerically that fluid velocity initially decreases with the increasing unsteadiness parameter, and temperature decreases significantly due to unsteadiness. Further, they found that the fluid velocity decreases with the increasing magnetic parameter. Increasing the Maxwell parameter values has the effect of suppressing the velocity field and increasing the temperature. In their study, they assumed that the magnetic Reynolds number is very small and that the electric field due to the polarization of charges is negligible. [9] studied the effects of magnetic field and nanoparticle on the Jeffery-Hamel flow of fluid through a divergent wedge. He analytically found that the rate of transport is considerably reduced with an increase in Hartmann number. This clearly indicates that the transverse magnetic field opposes the transport phenomenon.

[3] studied Jeffery-Hamel flow and found that the velocity increases with an increase in the wedge semi-angle for the case of a diverging conduit. The influence of Reynolds number Re and the wedge semi-angle is the same for a diverging wedge. There is an increase in the velocity for a converging wedge with an increase in wedge semi-angle. For converging conduit, Reynolds number Re results in an increase in the velocity which is opposite to that for diverging conduit. [12] studied the effects of thermal radiation in a two-dimensional and magnetohydrodynamic (MHD) flow of an incompressible non-Newtonian fluid in a convergent/divergent wedge and observed that the temperature is a decreasing function of thermal radiation.

In their study of MHD Jeffery-Hamel Nanofluid Flow in Non-Parallel Walls, [18] found semi-analytically that the velocity boundary layer thickness decreases with increasing Reynolds number and nanoparticle volume fraction, and increases with increasing Hartmann number. They found further that an increase in Reynolds number leads to an increase in the magnitude of the skin friction coefficient. Generally, when the magnetic field is imposed on the wedge, the velocity field is suppressed owing to the retarding effect of the Lorentz force. Thus, the presence of the magnetic field increases the momentum boundary layer thickness. Moreover, they found that the skin friction coefficient is an increasing function of Reynolds number, wedge angle and nanoparticle volume friction but a decreasing function of Hartmann number.

[1] studied the MHD Jeffery-Hamel flow in nanofluids using new Homotopy Analysis Method and found that an increase in Hartmann number increases the fluid velocity while an increase in Reynolds number decreases the fluid velocity for both viscous and nanofluid. [8] studied magnetohydrodynamic flow and heat transfer of copper-water nanofluid in a conduit with non-parallel walls considering different shapes of nanoparticles and found numerically that an increase in wedge angle and the Reynolds number results in backflow for diverging wedge case. This backflow can be reduced by applying a strong magnetic field. Moreover, the magnetic number increases the velocity of the fluid. [5] studied the Jeffery-Hamel flow of a non-Newtonian fluid and found that for a diverging wedge, an increase in wedge semi-angle and Reynolds number results to a decrease in the fluid velocity. For all these parameters, the maximum velocity is observed near the center of the conduit.

[10] studied the Jeffery-Hamel flow of non-Newtonian fluid with nonlinear viscosity and wall friction and found that the Newtonian normalized velocity gradually decreases with the tangential direction progress, an increase in the friction coefficient leads to a decrease in the normalized Newtonian velocity profile values, and an increase in the Reynolds number results to an increase in the normalized velocity function values.

In spite of all these studies, unsteady flow of non-Newtonian fluid inside a divergent conduit in presence of magnetic field has received little attention. Therefore, the present paper investigates the unsteady Jeffery-Hamel flow of an incompressible non-Newtonian fluid with nonlinear viscosity and skin friction in presence of a constant applied magnetic field perpendicular to the fluid motion. The study has been motivated by the need to gather useful information for engineering, technology, and industrial applications such as in MHD power generators and also the need to complement the current study on Magnetic Drug Targeting in cancer therapy. The effect of pertinent parameters on the flow fields is investigated.

The rest of the paper is organized as follows: section 2 presents the model formulation, mathematical analysis, and the numerical simulations of the corresponding model, section 3 presents the results of the study, and section 4 presents the conclusion of the study.

2. Mathematical formulation

We consider an unsteady two-dimensional laminar flow of an incompressible electrically conducting non-Newtonian fluid inside a divergent wedge (non-parallel walls) with nonlinear viscosity and skin friction in the presence of a constant applied magnetic field in the direction perpendicular to the fluid motion as shown in Figure 1. A cylindrical coordinate system (r, θ, z) is chosen with the origin at the center of the wedge. The z-direction is taken to be the length of the wedge and r direction is taken to be the coordinate axis perpendicular to the wall.

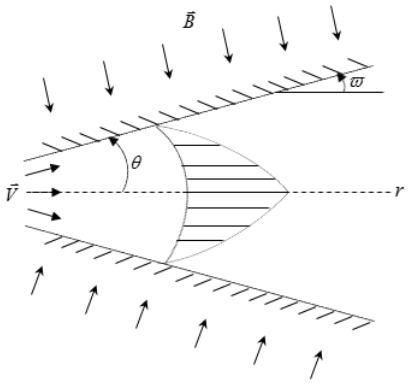

Figure 1: Geometry of the problem

It is assumed that the motion is purely radially dependent on r, θ, and t only. More-

over, the flow is unbounded in the z-direction (i.e., $\dfrac{\partial \Xi}{\partial z} = 0$), the tangential and perpendicular velocities are negligible (i.e., $u_\theta = u_z = 0$), and that the flow is stable and all body forces except magnetic field are neglected. Further, it is assumed that there is no chemical reaction taking place in the fluid, the viscosity is a function of wedge angle θ only, viscous dissipation is the source of energy, and that the thermal conductivity is constant. Also, it is assumed that the induced magnetic field is negligible in the flow field in comparison with the applied magnetic field, there is also no external electric field applied, so the effect of polarization of the fluid is negligible. Under the assumptions, the continuity, momentum, and energy equations governing the flow problem are elaborated here as follows:

The general equation of continuity for an unsteady flow, in vector notation, is given by:

$$\frac{\partial \rho}{\partial t} + \vec{\nabla} \cdot \left(\rho \vec{V}\right) = 0. \tag{1}$$

Under the assumptions, Eq. (1) reduces to

$$\frac{\partial}{\partial r}(r u_r) = 0, \tag{2}$$

where u_r and r represents the velocity vector and the radial velocity component, respectively.

The general equation of motion (equation of conservation of momentum) for an incompressible fluid flow, in vector notation, is given by:

$$\rho\Big(\frac{\partial \vec{V}}{\partial t} + \vec{V} \cdot \vec{\nabla}\vec{V}\Big) = -\vec{\nabla} p - \vec{\nabla} \cdot \vec{\tau} + \rho \vec{F}, \tag{3}$$

where $\vec{F}$, $\vec{\nabla} p$ and $\vec{\tau}$ represent the body forces, pressure gradient, and stress vector respectively. The stress vector represents six shear stresses (i.e., stresses acting in the direction of flow) and three normal stresses (i.e., compressive or tensile stresses perpendicular to the direction of flow). According to [16, 10], the components of the stress vector are generally defined by the following shear matrix:

$$\begin{pmatrix} \tau_{rr} & \tau_{r\theta} & \tau_{rz} \\ \tau_{\theta r} & \tau_{\theta\theta} & \tau_{\theta z} \\ \tau_{zr} & \tau_{z\theta} & \tau_{zz} \end{pmatrix} = \mu \begin{pmatrix} 2\dfrac{\partial u_r}{\partial r} - \dfrac{2}{3}\vec{\nabla} \cdot \vec{V} & \dfrac{1}{r}\dfrac{\partial u_r}{\partial \theta} + \dfrac{\partial u_\theta}{\partial r} - \dfrac{u_\theta}{r} & \dfrac{\partial u_z}{\partial r} + \dfrac{\partial u_r}{\partial z} \\ \dfrac{1}{r}\dfrac{\partial u_r}{\partial \theta} + \dfrac{\partial u_\theta}{\partial r} - \dfrac{u_\theta}{r} & 2\left(\dfrac{1}{r}\dfrac{\partial u_\theta}{\partial \theta} + \dfrac{u_r}{r}\right) - \dfrac{2}{3}\vec{\nabla} \cdot \vec{V} & \dfrac{\partial u_\theta}{\partial z} + \dfrac{1}{r}\dfrac{\partial u_z}{\partial \theta} \\ \dfrac{\partial u_z}{\partial r} + \dfrac{\partial u_r}{\partial z} & \dfrac{\partial u_\theta}{\partial z} + \dfrac{1}{r}\dfrac{\partial u_z}{\partial \theta} & 2\dfrac{\partial u_z}{\partial z} - \dfrac{2}{3}\vec{\nabla} \cdot \vec{V} \end{pmatrix},$$

where μ is the dynamic viscosity function. Under the assumptions, the shear matrix reduces to:

$$\begin{pmatrix} \tau_{rr} & \tau_{r\theta} & \tau_{rz} \\ \tau_{\theta r} & \tau_{\theta\theta} & \tau_{\theta z} \\ \tau_{zr} & \tau_{z\theta} & \tau_{zz} \end{pmatrix} = \mu \begin{pmatrix} 2\dfrac{\partial u_r}{\partial r} & \dfrac{1}{r}\dfrac{\partial u_r}{\partial \theta} & 0 \\ \dfrac{1}{r}\dfrac{\partial u_r}{\partial \theta} & 2\dfrac{u_r}{r} & 0 \\ 0 & 0 & 0 \end{pmatrix}. \tag{4}$$

Thus, the stress form of Eq. (3) in cylindrical coordinates is given by [16]

$$\begin{aligned}
\hat{r}: \quad & \rho\Big(\frac{\partial u_r}{\partial t}+u_r\frac{\partial u_r}{\partial r}+\frac{u_\theta}{r}\frac{\partial u_r}{\partial \theta}+u_z\frac{\partial u_r}{\partial z}-\frac{u_\theta^2}{r}\Big)=-\frac{\partial p}{\partial r}\\
&+\frac{1}{r}\frac{\partial}{\partial r}(r\tau_{rr})+\frac{1}{r}\frac{\partial \tau_{r\theta}}{\partial \theta}+\frac{\partial \tau_{rz}}{\partial z}-\frac{\tau_{\theta\theta}}{r}+\rho F_r\\
\hat{\theta}: \quad & \rho\Big(\frac{\partial u_\theta}{\partial t}+u_r\frac{\partial u_\theta}{\partial r}+\frac{u_\theta}{r}\frac{\partial u_\theta}{\partial \theta}+u_z\frac{\partial u_\theta}{\partial z}+\frac{u_r u_\theta}{r}\Big)=-\frac{1}{r}\frac{\partial p}{\partial \theta}\\
&+\frac{1}{r^2}\frac{\partial}{\partial r}(r^2\tau_{\theta r})+\frac{1}{r}\frac{\partial \tau_{\theta\theta}}{\partial \theta}+\frac{\partial \tau_{\theta z}}{\partial z}+\rho F_\theta\\
\hat{k}: \quad & \rho\Big(\frac{\partial u_z}{\partial t}+u_r\frac{\partial u_z}{\partial r}+\frac{u_\theta}{r}\frac{\partial u_z}{\partial \theta}+u_z\frac{\partial u_z}{\partial z}\Big)=-\frac{\partial p}{\partial z}+\frac{1}{r}\frac{\partial}{\partial r}(r\tau_{zr})+\frac{1}{r}\frac{\partial \tau_{z\theta}}{\partial \theta}+\frac{\partial \tau_{zz}}{\partial z}+\rho F_z
\end{aligned} \quad , \tag{5}$$

where F_r, F_θ, and F_z are the components of the body force per unit mass of the fluid in the r,θ, and z-direction respectively.

By Ohm's law, the electric current density induced in the conductive fluid is generally given by (without taking Hall current into account):

$$\vec{J}=\sigma\left(\vec{E}+\vec{V}\times\vec{B}\right),$$

where σ denotes the electrical conductivity of the fluid, $\vec{B}$ is the magnetic field, $\vec{E}$ is the electric field, and $\vec{V}$ is the velocity vector. Simultaneously occurring with the induced current is the Lorentz force (i.e., total electromagnetic force) $\vec{F}$ given by

$$\vec{F}=\frac{1}{\rho}\left(\rho_e\vec{E}+\vec{J}\times\vec{B}\right).$$

In our flow problem, the electrostatic force $\rho_e\vec{E}$ is negligibly small as compared to the electromagnetic force $\vec{J}\times\vec{B}$ since there is no externally applied electric current. Hence,

$$\vec{F}=\frac{1}{\rho}\left(\vec{J}\times\vec{B}\right)=\frac{\sigma}{\rho}(\vec{V}\times\vec{B})\times\vec{B}=\frac{\sigma}{\rho}\big[[\vec{B}\cdot\vec{V}]\vec{B}-[\vec{B}\cdot\vec{B}]\vec{V}\big].$$

Since the magnetic field is applied in a direction perpendicular to the fluid motion, then $\vec{B}\cdot\vec{V}=0$. Furthermore, $\vec{B}=(B_0,0,0)$ and $\vec{V}=(u_r,0,0)$. Thus the body force $\vec{F}$ becomes:

$$\vec{F}=-\frac{\sigma}{\rho}\big[[\vec{B}\cdot\vec{B}]\vec{V}\big]=-\frac{\sigma}{\rho}B_0^2u_r\hat{r}. \tag{6}$$

Under the assumptions, Eq. (5) reduces to the following radial and tangential displacement equation, respectively:

$$\begin{aligned}
\hat{r}: \quad & \rho\Big(\frac{\partial u_r}{\partial t}+u_r\frac{\partial u_r}{\partial r}\Big)=-\frac{\partial p}{\partial r}+\frac{1}{r}\frac{\partial}{\partial r}(r\tau_{rr})+\frac{1}{r}\frac{\partial \tau_{r\theta}}{\partial \theta}-\frac{\tau_{\theta\theta}}{r}-\sigma B_0^2u_r\\
\hat{\theta}: \quad & 0=-\frac{1}{r}\frac{\partial p}{\partial \theta}+\frac{1}{r^2}\frac{\partial}{\partial r}(r^2\tau_{\theta r})+\frac{1}{r}\frac{\partial \tau_{\theta\theta}}{\partial \theta}
\end{aligned} \quad . \tag{7}$$

From Eqs. (4) and (7) we obtain:

$$\begin{aligned} \hat{r}: \quad & \rho\left(\frac{\partial u_r}{\partial t}+u_r\frac{\partial u_r}{\partial r}\right)=-\frac{\partial p}{\partial r}+\frac{1}{r}\frac{\partial}{\partial r}\left(2\mu r\frac{\partial u_r}{\partial r}\right)+\frac{1}{r}\frac{\partial}{\partial \theta}\left(\frac{\mu}{r}\frac{\partial u_r}{\partial \theta}\right)-2\mu\frac{u_r}{r^2}-\sigma B_0^2 u_r \\ \hat{\theta}: \quad & 0=-\frac{1}{r}\frac{\partial p}{\partial \theta}+\frac{1}{r^2}\frac{\partial}{\partial r}\left(\mu r\frac{\partial u_r}{\partial \theta}\right)+\frac{1}{r}\frac{\partial}{\partial \theta}\left(2\mu\frac{u_r}{r}\right) \end{aligned} . \tag{8}$$

Thus, Eq. (8) reduces to

$$\hat{r}: \quad \rho\frac{\partial u_r}{\partial t}=-\frac{\partial p}{\partial r}+2\frac{\partial \mu}{\partial r}\frac{\partial u_r}{\partial r}+\frac{1}{r^2}\frac{\partial \mu}{\partial \theta}\frac{\partial u_r}{\partial \theta}+\mu\left(\frac{1}{r^2}\frac{\partial^2 u_r}{\partial \theta^2}+2\frac{\partial^2 u_r}{\partial r^2}+\frac{2}{r}\frac{\partial u_r}{\partial r}-2\frac{u_r}{r^2}\right)$$

$$-\rho u_r\frac{\partial u_r}{\partial r}-\sigma B_0^2 u_r \tag{9}$$

$$\hat{\theta}: \quad -\frac{1}{r}\frac{\partial p}{\partial \theta}+\frac{1}{r}\frac{\partial \mu}{\partial r}\frac{\partial u_r}{\partial \theta}+\mu\left(\frac{3}{r^2}\frac{\partial u_r}{\partial \theta}+\frac{1}{r}\frac{\partial^2 u_r}{\partial r\partial \theta}\right)+2\frac{u_r}{r^2}\frac{\partial \mu}{\partial \theta}=0. \tag{10}$$

The foregoing Eqs. (9) and (10) represent the equation of motion in cylindrical coordinates for the unsteady two-dimensional laminar flow of an incompressible fluid whose motion is assumed to be symmetrical and purely radial.

Differentiating Eq. (2) along the radial direction yields

$$\frac{\partial^2 u_r}{\partial r^2}+\frac{1}{r}\frac{\partial u_r}{\partial r}-\frac{u_r}{r^2} \;=\; 0. \tag{11}$$

From Eqs. (9) and (11), we obtain:

$$\hat{r}: \ \rho\frac{\partial u_r}{\partial t}=-\frac{\partial p}{\partial r}+2\frac{\partial \mu}{\partial r}\frac{\partial u_r}{\partial r}+\frac{1}{r^2}\frac{\partial \mu}{\partial \theta}\frac{\partial u_r}{\partial \theta}+\frac{\mu}{r^2}\frac{\partial^2 u_r}{\partial \theta^2}-\rho u_r\frac{\partial u_r}{\partial r}-\sigma B_0^2 u_r. \tag{12}$$

Differentiating Eq. (2) along the tangential direction yields

$$\frac{\partial^2 u_r}{\partial r\partial \theta}+\frac{1}{r}\frac{\partial u_r}{\partial \theta}=0. \tag{13}$$

From Eqs. (10) and (13), we obtain:

$$\hat{\theta}: \ -\frac{\partial p}{\partial \theta}+\frac{\partial \mu}{\partial r}\frac{\partial u_r}{\partial \theta}+2\frac{\mu}{r}\frac{\partial u_r}{\partial \theta}+2\frac{u_r}{r}\frac{\partial \mu}{\partial \theta}=0. \tag{14}$$

Differentiating Eq. (12) along the tangential direction and rearranging we obtain

$$\begin{aligned} \hat{r}: \ \frac{\partial^2 p}{\partial r\partial \theta} \;=\; & -\rho\frac{\partial^2 u_r}{\partial \theta\partial t}+2\frac{\partial^2 \mu}{\partial r\partial \theta}\frac{\partial u_r}{\partial r}+2\frac{\partial \mu}{\partial r}\frac{\partial^2 u_r}{\partial r\partial \theta}+\frac{1}{r^2}\frac{\partial^2 \mu}{\partial \theta^2}\frac{\partial u_r}{\partial \theta}+\frac{1}{r^2}\frac{\partial \mu}{\partial \theta}\frac{\partial^2 u_r}{\partial \theta^2} \\ & +\frac{1}{r^2}\frac{\partial \mu}{\partial \theta}\frac{\partial^2 u_r}{\partial \theta^2}+\frac{\mu}{r^2}\frac{\partial^3 u_r}{\partial \theta^3}-\rho\frac{\partial u_r}{\partial \theta}\frac{\partial u_r}{\partial r}-\rho u_r\frac{\partial^2 u_r}{\partial r\partial \theta}-\sigma B_0^2\frac{\partial u_r}{\partial \theta}. \end{aligned} \tag{15}$$

Differentiating Eq. (14) along the radial direction and rearranging we obtain:

$$\hat{\theta}: \frac{\partial^2 p}{\partial r \partial \theta} = \frac{\partial^2 \mu}{\partial r^2}\frac{\partial u_r}{\partial \theta} + \frac{\partial \mu}{\partial r}\frac{\partial^2 u_r}{\partial r \partial \theta} - 2\frac{\mu}{r^2}\frac{\partial u_r}{\partial \theta} + \frac{2}{r}\frac{\partial \mu}{\partial r}\frac{\partial u_r}{\partial \theta} + 2\frac{\mu}{r}\frac{\partial^2 u_r}{\partial r \partial \theta} - 2\frac{u_r}{r^2}\frac{\partial \mu}{\partial \theta} + \frac{2}{r}\frac{\partial u_r}{\partial r}\frac{\partial \mu}{\partial \theta} + 2\frac{u_r}{r}\frac{\partial^2 \mu}{\partial r \partial \theta}. \quad (16)$$

Eliminating the term containing p between Eqs. 15 and (16), we obtain the following nonlinear partial differential equation:

$$\frac{\partial^2 u_r}{\partial \theta \partial t} = \frac{2}{\rho}\frac{\partial^2 \mu}{\partial r \partial \theta}\frac{\partial u_r}{\partial r} + \frac{2}{\rho}\frac{\partial \mu}{\partial r}\frac{\partial^2 u_r}{\partial r \partial \theta} + \frac{1}{\rho r^2}\frac{\partial^2 \mu}{\partial \theta^2}\frac{\partial u_r}{\partial \theta} + \frac{\partial \mu}{\partial \theta}\left(\frac{2}{\rho r^2}\frac{\partial^2 u_r}{\partial \theta^2} + 2\frac{u_r}{\rho r^2} - \frac{2}{\rho r}\frac{\partial u_r}{\partial r}\right) + \frac{\mu}{\rho}\left(\frac{1}{r^2}\frac{\partial^3 u_r}{\partial \theta^3} + \frac{2}{r^2}\frac{\partial u_r}{\partial \theta} - \frac{2}{r}\frac{\partial^2 u_r}{\partial r \partial \theta}\right) - \frac{\partial u_r}{\partial \theta}\frac{\partial u_r}{\partial r} - u_r\frac{\partial^2 u_r}{\partial r \partial \theta} - \frac{1}{\rho}\frac{\partial^2 \mu}{\partial r^2}\frac{\partial u_r}{\partial \theta} - \frac{1}{\rho}\frac{\partial \mu}{\partial r}\frac{\partial^2 u_r}{\partial r \partial \theta} - \frac{2}{\rho r}\frac{\partial \mu}{\partial r}\frac{\partial u_r}{\partial \theta} - 2\frac{u_r}{\rho r}\frac{\partial^2 \mu}{\partial r \partial \theta} - \frac{\sigma B_0^2}{\rho}\frac{\partial u_r}{\partial \theta}. \quad (17)$$

The foregoing Eq. (17) is the reduced form of the equation of motion in cylindrical coordinates for the unsteady two-dimensional laminar flow of an incompressible fluid whose motion is symmetrical and purely radial.

The general equation of energy for an incompressible fluid, in vector notation, is given by [16]

$$\rho C_p\left(\frac{\partial T}{\partial t} + \vec{V}\cdot\vec{\nabla}T\right) = \rho\dot{q}_g + \vec{\nabla}\cdot(k\vec{\nabla}T) + \beta T\frac{D\rho}{Dt} + \Phi, \quad (18)$$

where Φ is the viscous dissipation rate. According to [16], Eq. (18) in cylindrical coordinates for an incompressible fluid with constant thermal conductivity k is given by (neglecting the force due to gravity):

$$\rho C_p\left(\frac{\partial T}{\partial t} + u_r\frac{\partial T}{\partial r} + \frac{u_\theta}{r}\frac{\partial T}{\partial \theta} + u_z\frac{\partial T}{\partial z}\right) = k\left[\frac{1}{r}\frac{\partial}{\partial r}\left(r\frac{\partial T}{\partial r}\right) + \frac{1}{r^2}\frac{\partial^2 T}{\partial \theta^2} + \frac{\partial^2 T}{\partial z^2}\right] + \Phi, \quad (19)$$

where the viscous dissipation rate, Φ, is given by the following expression:

$$\Phi = 2\mu\left[\left(\frac{\partial u_r}{\partial r}\right)^2 + \left(\frac{1}{r}\frac{\partial u_\theta}{\partial \theta} + \frac{u_r}{r}\right)^2 + \left(\frac{\partial u_z}{\partial z}\right)^2\right] + \mu\left[\left(\frac{1}{r}\frac{\partial u_r}{\partial \theta} + \frac{\partial u_\theta}{\partial r} - \frac{u_\theta}{r}\right)^2 + \left(\frac{\partial u_\theta}{\partial z} + \frac{1}{r}\frac{\partial u_z}{\partial \theta}\right)^2 + \left(\frac{\partial u_z}{\partial r} + \frac{\partial u_r}{\partial z}\right)^2\right].$$

The dissipation function, Φ, is non-negative since it only consists of squared terms and represents a source of internal energy due to deformation work on the fluid particles. The deformation work is extracted from the mechanical activity which causes the motion and is converted into internal energy or heat.

Under the assumptions, Eq. (19) reduces to:

$$\frac{\partial T}{\partial t} = \alpha\left[\frac{1}{r}\frac{\partial T}{\partial r} + \frac{\partial^2 T}{\partial r^2} + \frac{1}{r^2}\frac{\partial^2 T}{\partial \theta^2}\right] - u_r\frac{\partial T}{\partial r} + \frac{\mu}{\rho C_p}\left[2\left(\frac{\partial u_r}{\partial r}\right)^2 + 2\left(\frac{u_r}{r}\right)^2 + \left(\frac{1}{r}\frac{\partial u_r}{\partial \theta}\right)^2\right], \quad (20)$$

where $\alpha = \dfrac{k}{\rho C_p}$ is the thermal diffusivity. The foregoing Eq. (20) represents the equation of energy in cylindrical coordinates for the unsteady two-dimensional laminar flow of an incompressible fluid whose motion is assumed to be symmetrical and purely radial; with constant thermal conductivity.

The boundary conditions for this flow problem are [8]:

$$\begin{cases} \text{At the centerline: } u_r = U_\infty, \dfrac{\partial u_r}{\partial \theta} = 0,\ T = T_\infty, \dfrac{\partial T}{\partial \theta} = 0 & \text{at } \theta = 0 \\ \text{On the walls: } \dfrac{\partial u_r}{\partial \theta} = -\gamma U(\theta),\ T = T_w & \text{at } \theta = \varpi \end{cases}, \quad (21)$$

where U_∞ is the centerline velocity, $\gamma \geq 0$ represents the friction coefficient factor. The boundary is said to be smooth if $\gamma = 0$, and perfectly rough if $\gamma \to \infty$. Here, ϖ represents the wedge semi-angle where the interval $-|\varpi| < \theta < |\varpi|$ is the flow field domain. If we require that the volumetric flow rate $Q \geq 0$, then, for $\varpi > 0$, the flow is diverging from a source at $\theta = 0$. Since the model consists of nonlinear partial differential equations (PDEs) i.e., Eqs. (17) and (20), it is convenient to reduce them to ordinary differential equations (ODEs) by the use of similarity transformation since the solution of ODEs are usually simpler and easier. The continuity equation (2) is automatically satisfied by introducing a stream function $\Psi(r, \theta, t)$ as,

$$\frac{\partial \Psi}{\partial \theta} = r u_r,\ \frac{\partial \Psi}{\partial r} = 0. \quad (22)$$

Therefore, Eq. (22) can be written as:

$$r u_r = f(\theta, t).$$

Letting $f(\theta, t) = -Q\dfrac{1}{\delta^{m+1}}F(\theta)$, we obtain the following transformation for the fluid velocity.

$$u_r = -\frac{Q}{r}\frac{1}{\delta^{m+1}}F(\theta), \quad (23)$$

where F is the dimensionless stream function, m is an arbitrary constant and is related to the wedge angle, and δ is the time-dependent length scale.

From the power-law model i.e., $\mu = \mu_0\left(\dfrac{du}{dy}\right)^{n-1}$, letting the velocity gradient $\dfrac{du}{dy}$ to be $g(\theta)$ we obtain the following transformation for the apparent viscosity:

$$\mu = \mu_0 g^{n-1}(\theta). \quad (24)$$

It is important to note that the velocity gradient is a function of θ only since we found from the continuity equation that the stream function Ψ is independent of r.

The similarity transformation for the temperature distribution is given by:

$$\frac{\omega(\theta)}{\delta^{m+1}} = \frac{T - T_w}{T_\infty - T_w}. \tag{25}$$

From Eqs. (17), (20), (23), (24), and (25), we obtain the following ordinary differential equations:

$$\begin{aligned}&(n-1)\left[(n-2)g^{n-3}g'^2 + g^{n-2}g''\right]F' + (n-1)g^{n-2}g'\left[2F'' + 4F\right]\\ &+g^{n-1}\left[F''' + 4F'\right] - 2Re\frac{1}{\delta^{m+1}}FF' - Ha^2F' + (m+1)\frac{r^{m+1}}{\delta^{m+1}}\lambda F' = 0\end{aligned} \tag{26}$$

and

$$\frac{1}{Pr}\omega'' + (m+1)\frac{r^{m+1}}{\delta^{m+1}}\lambda\omega + \frac{Ec}{\delta^{m+1}}g^{n-1}\left[4F^2 + F'^2\right] = 0, \tag{27}$$

where $Re = \dfrac{Q\rho}{\mu_0}$ is the Reynolds number, $Ha = B_0 r\left(\dfrac{\sigma}{\mu_0}\right)^{\frac{1}{2}}$ is the Hartmann number, $Pr = \dfrac{\mu_0}{\rho\alpha}$ is the Prandtl number, $Ec = \dfrac{Q^2/r^2}{C_p(T_\infty - T_w)}$ is the Eckert number, and $\lambda = \dfrac{\rho\delta^m}{\mu_0 r^{m-1}}\dfrac{d\delta}{dt}$ is the unsteadiness parameter. The prime denotes the differentiation with respect to θ.

In order to simplify solutions, we consider the following expression for the velocity gradient:

$$g = \theta^c,\ c \geq 2,$$

Thus Eqs. (26) and (27) reduce to:

$$\begin{aligned}&c(n-1)\theta^{c(n-1)-2}\left[c(n-1)-1\right]F' + c(n-1)\theta^{c(n-1)-1}\left[2F'' + 4F\right]\\ &+\theta^{c(n-1)}\left[F''' + 4F'\right] - 2Re\frac{1}{\delta^{m+1}}FF' - Ha^2F' + (m+1)\frac{r^{m+1}}{\delta^{m+1}}\lambda F' = 0,\end{aligned} \tag{28}$$

and

$$\frac{1}{Pr}\omega'' + (m+1)\frac{r^{m+1}}{\delta^{m+1}}\lambda\omega + \frac{Ec}{\delta^{m+1}}\theta^{c(n-1)}\left[4F^2 + F'^2\right] = 0. \tag{29}$$

Therefore, Eqs. (28) and (29) are the final set of the model equations in dimensionless form. The corresponding boundary conditions are:

$$\begin{cases}\text{At the centerline: } F(0) = 1,\ F'(0) = 0,\ \omega(0) = \delta^{m+1} & \text{at } \theta = 0\\ \text{On the walls: } F'(\varpi) = -\gamma F(\varpi),\ \omega(0) = 0 & \text{at } \theta = \varpi\end{cases}. \tag{30}$$

2.1. Numerical solution

In most cases, equations governing scientific problems such as Jeffery-Hamel flow of non-Newtonian fluids and other fluid mechanic problems are inherently in the form of nonlinear differential equations. Due to the nonlinearity of the resulting equations, an analytical solution is not possible. Therefore, these nonlinear equations are solved using approximation methods (i.e., numerical techniques or semi-analytical methods) in order to accomplish non-analytical solutions [3]. The semi-analytical methods include Homotopy Perturbation Method (HPM), Homotopy Analysis Method (HAM) and Differential Transform Method (DTM) . However, most of these semi-analytical techniques are either very difficult to employ and require a lot of computation or the level of accuracy has to be compromised; which not only affects the results badly but (in some cases) they become completely unreliable [6]. Therefore, the governing equations (28) and (29) subject to the boundary conditions (30) were solved numerically by collocation method. Collocation method is a numerical technique that estimates the solution using a polynomial and makes use of solvers that take low computational memory. Furthermore, the collocation method is easy to program. Hence, it is more advantageous to use in boundary value problems than other numerical techniques.

Thus adopting the collocation technique, a computer program was set up for the solution of the governing coupled nonlinear ordinary differential equations of our flow problem with the aid of the inbuilt MATLAB function known as bvp4c. The bvp4c algorithm has been well tested for its accuracy and robustness. A detailed explanation of the Collocation method for MATLAB implementation can be found in [17].

2.1.1 Computing the skin-friction coefficient and rate of heat transfer

The parameters of engineering interest for the present problem are the local skin-friction coefficient and wall heat transfer rate. These can be obtained from the following expressions [14]. Skin friction coefficient;

$$C_f = \frac{2}{\sqrt{Re(2-\varepsilon)}} F'(0)$$

and Nusselt number;

$$N_u = -\sqrt{\frac{Re}{(2-\varepsilon)}}\omega'(0),$$

where $\varepsilon = \dfrac{2m}{m+1}$ is the wedge angle parameter that corresponds to $2\varpi = \varepsilon\pi$ for a total angle 2ϖ of the wedge.

3. Results and discussion

Numerical values of velocity and temperature are presented graphically for different values of the Reynolds number $Re \in [3, 25]$, Hartman number $Ha \in [0.5, 5]$, Prandtl number $Pr \in [0.5, 5]$, Eckert number $Ec \in [2, 10]$, and unsteadiness parameter $\lambda \in [1.5, 15]$.

The effects of varying the flow parameters such as Reynolds number, Hartmann number, Prandtl number, and Eckert number; and unsteadiness parameter on the dimensionless flow variables such as velocity and temperature have been determined using simulation. The other parameters such as wedge angle ϖ, flow behavior index n, friction coefficient factor γ, time-dependent length scale δ, and the constants c and m are kept constant throughout. The results are presented in form of graphs and tables as follows:

3.1. Effects of Varying Reynolds number on Velocity and Temperature Profiles

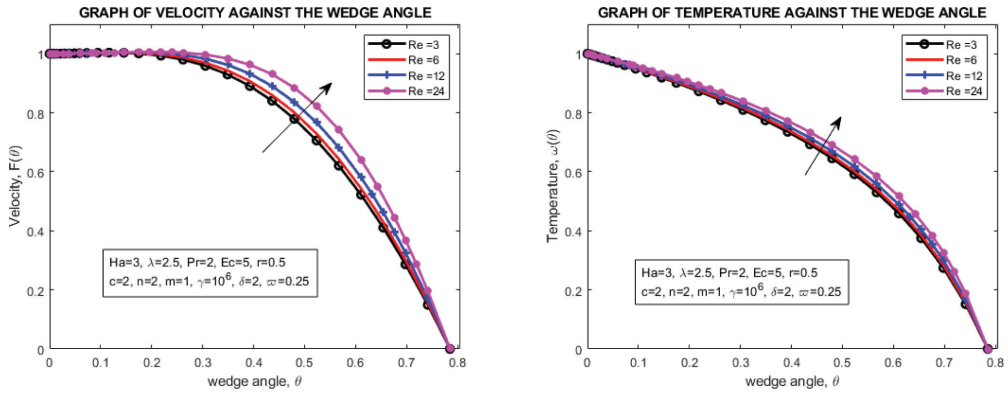

(a) Velocity profile (b) Temperature profile

Figure 2: Plots of dimensionless velocity and temperature for different values of Reynolds number Re.

From Figure 2(a), it is noted that an increase in the values of the Reynolds number leads to an increase in the fluid velocity. This is because Reynolds number expresses the relationship between inertial force and viscous force. Thus, a small Reynolds number implies that the viscous force is predominant and as a result, there will be a retardation of the flow due to the formation and extension of the boundary layer into the flow region. Conversely, a large value of Reynolds number implies that the viscous force is less predominant and as a result, there will be less retardation of the flow since the boundary layer formed does not really extend into the flow region.

From Figure 2(b), it is noted that an increase in the values of the Reynolds number leads to an increase in the fluid temperature. This is because an increase in the Reynolds number means that the viscous force becomes less predominant and hence the fluid viscosity decreases. Since viscosity and temperature are inversely proportional in liquids, a decrease in viscosity implies an increase in the fluid temperature.

3.2. Effects of Varying Hartman number on Velocity and Temperature Profiles

From Figure 3(a), it is noted that an increase in the values of the Hartmann number leads to an increase in the fluid velocity. This is because Hartmann number expresses the relationship between electromagnetic force and viscous force. Thus, the application of a magnetic field moving with the free stream has the tendency to induce an electromotive

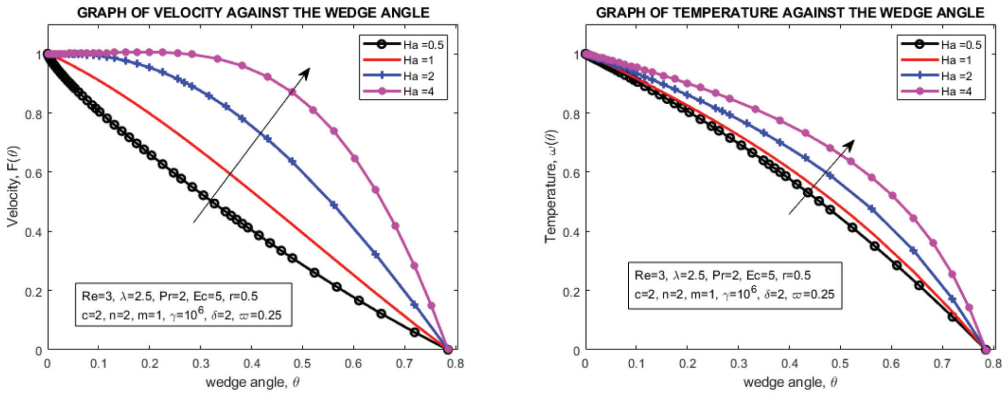

(a) Velocity profile (b) Temperature profile

Figure 3: Plots of dimensionless velocity and temperature for different values of Hartmann number Ha.

force known as the Lorentz force which decreases the hydrodynamic boundary layer thickness. So, increasing the value of the Hartmann number means that the magnetic force is predominant and since this force is in the direction of the fluid flow, it accelerates the transport phenomena.

From Figure 3(b), it is noted that an increase in the values of the Hartmann number leads to an increase in the fluid temperature. This is because an increase in the Hartman number means that the magnetic force is predominant. This force increases the thermal boundary layer thickness and hence increasing the fluid temperature.

3.3. Effects of Varying Prandtl number on Velocity and Temperature Profiles

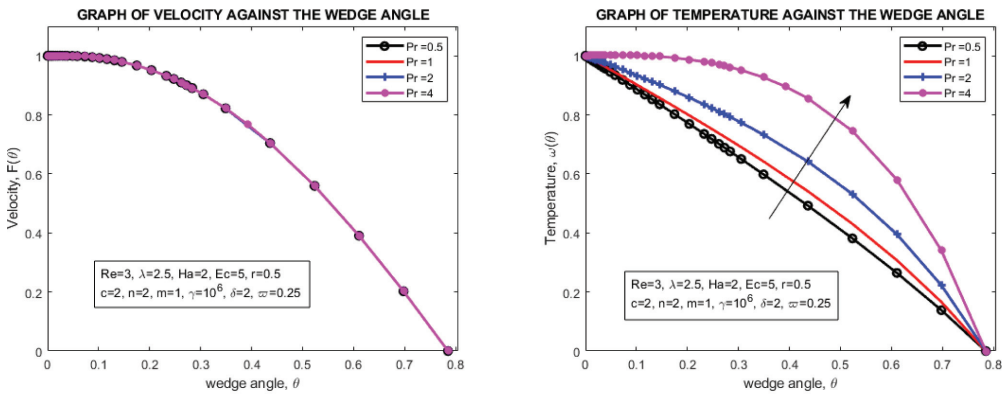

(a) Velocity profile (b) Temperature profile

Figure 4: Plots of dimensionless velocity and temperature for different values of Prandtl number Pr.

From Figure 4(a), it is noted that an increase in the values of the Prandtl number doesn't lead to a change in the fluid velocity. Furthermore, it is noted from Figure 4(b)

that an increase in the values of the Prandtl number leads to an increase in the fluid temperature. This is because Prandtl number expresses the relationship between momentum diffusivity and thermal diffusivity. Thus, an increase in the Prandtl number means that the momentum diffusivity is high. The momentum transfer consequently yields heat transfer. So, the kinetic energy gained weakens the viscous force between the layers of the fluid. This yields a decrease in the fluid viscosity and as a result, increasing the fluid temperature.

3.4. Effects of Varying Eckert number on Velocity and Temperature Profiles

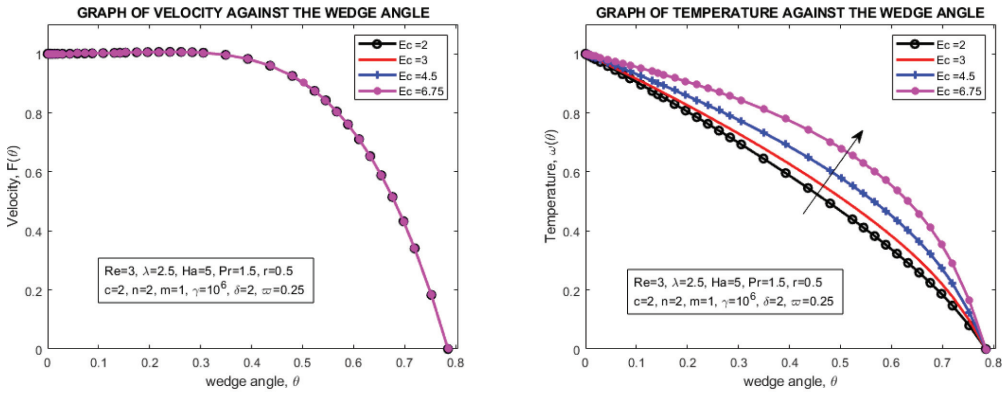

(a) Velocity profile (b) Temperature profile

Figure 5: Plots of dimensionless velocity and temperature for different values of Eckert number Ec.

From Figure 5(a), it is noted that an increase in the values of the Eckert number doesn't lead to a change in the fluid velocity. Furthermore, it is noted from Figure 5(b) that an increase in the values of the Eckert number leads to an increase in the fluid temperature. This is because Eckert number expresses the relationship between heat dissipation potential and advective transport. Thus, an increase in the Eckert number means that the heat dissipation potential also increases. This leads to an increase in the thermal boundary layer thickness and hence, increasing the fluid temperature.

3.5. Effects of Varying the Unsteadiness Parameter on Velocity and Temperature Profiles

From Figure 6(a), it is noted that an increase in the values of the unsteadiness parameter leads to a decrease in the fluid velocity. This is because an increase in the unsteadiness parameter implies that the boundary tends to be nearer to the centerline. So, the presence of the frictional force increases the drag between the boundary and the fluid particles and as a result, forming a boundary layer which extends into the flow region. Hence, this retards the transport phenomena.

From Figure 6(b), it is noted that an increase in the values of the unsteadiness parameter leads to an increase in the fluid temperature. This is due to the fact that there

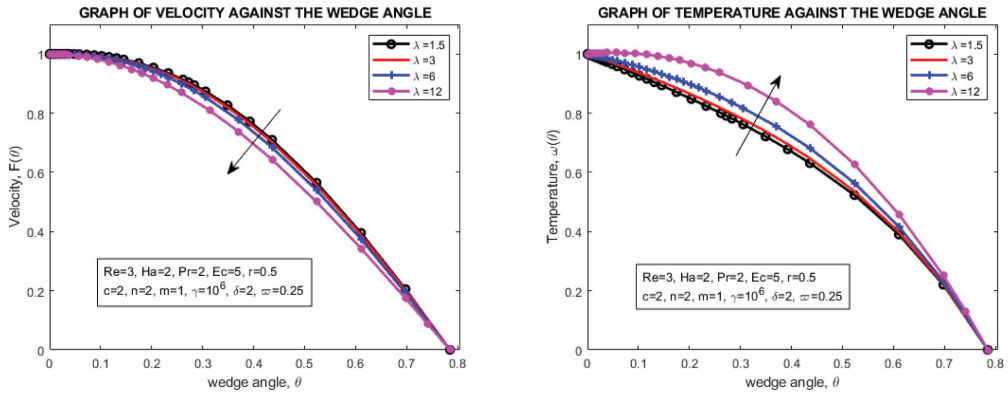

(a) Velocity profile (b) Temperature profile

Figure 6: Plots of dimensionless velocity and temperature for different values of unsteadiness parameter λ.

is viscous dissipation taking place in the fluid as it flows i.e., the fluid viscosity takes kinetic energy from the motion of the fluid and converts it into heat. This heats up the fluid and so as time increases, the system acquires more heat and hence increasing the fluid temperature.

3.6. Effect of parameters on skin friction coefficient and rate of heat transfer

The quantities of practical interest in this study are the skin friction coefficient and the rate of heat transfer. The local skin-friction coefficient and the local Nusselt number which are respectively proportional to $-F'(0)$ and $-\omega'(0)$ are computed and their numerical values presented in tabular form.

The results of varying parameter value on the local skin-friction coefficient and the local Nusselt number are shown in Table 1. It is noted that the skin friction coefficient increases with increasing values of the unsteadiness parameter λ, it decreases with increasing values of the Reynolds number and Hartmann number, and it remains constant with increasing values of the Prandtl number and Eckert number. Moreover, the rate of heat transfer increases with increasing values of Reynolds number and it decreases with increasing values of Hartmann number, Prandtl number, Eckert number, and unsteadiness parameter.

4. Conclusion

Based on the obtained graphical and tabular results, the following major conclusions have been drawn:

- The fluid velocity increases with increasing values of the Reynolds number and Hartmann number. The velocity, however, decreases with increasing values of

Table 1: Skin friction coefficient and rate of heat transfer for different values of the parameters Re, Ha, Pr, Ec, and λ

Re	Ha	Pr	Ec	λ	C_f	N_u
3	3	2	5	2.5	1.0745×10^{-8}	0.8822
6	3	2	5	2.5	5.5941×10^{-9}	1.2001
12	3	2	5	2.5	2.5897×10^{-9}	1.5872
24	3	2	5	2.5	4.8740×10^{-9}	2.0214
3	0.5	2	5	2.5	-79.9781	1.5626
3	1	2	5	2.5	-0.4556	1.3985
3	2	2	5	2.5	3.9206×10^{-7}	1.0894
3	4	2	5	2.5	4.0219×10^{-9}	0.7472
3	2	0.5	5	2.5	3.9196×10^{-7}	1.9359
3	2	1	5	2.5	3.9196×10^{-7}	1.6602
3	2	2	5	2.5	3.9196×10^{-7}	1.0894
3	2	4	5	2.5	3.9196×10^{-7}	-0.1360
3	2	1.5	2	2.5	8.2165×10^{-5}	1.6165
3	2	1.5	3	2.5	8.2165×10^{-5}	1.4303
3	2	1.5	4.5	2.5	8.2165×10^{-5}	1.1512
3	2	1.5	6.75	2.5	8.2165×10^{-5}	0.7324
3	2	2	5	1.5	2.9528×10^{-7}	1.2175
3	2	2	5	3	4.5260×10^{-7}	1.0244
3	2	2	5	6	1.0747×10^{-6}	0.6200
3	2	2	5	12	-4.6420×10^{-8}	-0.2733

the unsteadiness parameter, and it remains constant with increasing values of the Prandtl number and Eckert number.

- The fluid temperature increases with increasing values of the Reynolds number, Hartmann number, Prandtl number, Eckert number, and unsteadiness parameter.
- The skin-friction coefficient increases with increasing values of the unsteadiness parameter. The skin-friction coefficient, however, decreases with increasing values of the Reynolds number and Hartmann number, and it remains constant with increasing values of the Prandtl number and Eckert number.
- The rate of heat transfer increases with increasing values of Reynolds number. It, however, decreases with increasing values of the Hartmann number, Prandtl number, Eckert number, and unsteadiness parameter.

Declaration of conflicting interests

The authors declare that there are no potential conflicts of interest regarding the research, authorship, and publication of this paper.

Acknowledgement

Our thanks to both the African Union Commission (AUC) and Japan International Cooperation Agency (JICA) for the financial support they extended to us in the research, authorship, and publication of this paper.

References

[1] V Ananthaswamy and N Yogeswari. A study on mhd jeffery–hamel flow in nanofluids using new homotopy analysis method. *International Journal of Scientific Research and Modern Education*, 1(1):2455–5630, 2016.

[2] Emmanuel Maurice Arthur, Ibrahim Yakubu Seini, and Letis Bortey Bortteir. Analysis of casson fluid flow over a vertical porous surface with chemical reaction in the presence of magnetic field. *Journal of Applied Mathematics and Physics*, 3(06):713, 2015.

[3] DR G Domairry, A Mohsenzadeh, and M Famouri. The application of homotopy analysis method to solve nonlinear differential equation governing jeffery–hamel flow. *Communications in Nonlinear Science and Numerical Simulation*, 14(1):85–95, 2009.

[4] AA Imani, Y Rostamian, DD Ganji, and HB Rokni. Analytical investigation of jeffery-hamel flow with high magnetic field and nano particle by rvim. *International Journal of Engineering*, 25(3):249–256, 2012.

[5] Umar Khan, Naveed Ahmed, Waseem Sikandar, and Syed Tauseef Mohyud-Din. Jeffery hamel flow of a non-newtonian fluid. *Journal of Applied and Computational Mechanics*, 2(1):21–28, 2016.

[6] Umar Khan, Naveed Ahmed, ZA Zaidi, SU Jan, and Syed Tauseef Mohyud-Din. On jeffery–hamel flows. *Int. J. Mod. Math. Sci*, 7:236–247, 2013.

[7] WA Manyonge, DW Kiema, and CCW Iyaya. Steady mhd poiseuille flow between two infinite parallel porous plates in an inclined magnetic field. *Int J Pure Appl Math*, 76(5):661–668, 2012.

[8] Syed Tauseef Mohyud-Din, Umar Khan, and Saleh M Hassan. Numerical investigation of magnetohydrodynamic flow and heat transfer of copper–water nanofluid in a channel with non-parallel walls considering different shapes of nanoparticles. *Advances in Mechanical Engineering*, 8(3):1687814016637318, 2016.

[9] Swati Mukhopadhyay. Heat transfer analysis of the unsteady flow of a maxwell fluid over a stretching surface in the presence of a heat source/sink. *Chinese Physics Letters*, 29(5):054703, 2012.

[10] J Nagler. Jeffery-hamel flow of non-newtonian fluid with nonlinear viscosity and wall friction. *Applied Mathematics and Mechanics*, 38(6):815–830, 2017.

[11] Quoc-Hung Nguyen and Ngoc-Diep Nguyen. Incompressible non-newtonian fluid flows. In *Continuum Mechanics-Progress in fundamentals and Engineering applications*. InTech, 2012.

[12] Hamed Ziaei Poor, Hassan Moosavi, Amir Moradi, and Mahboubeh Parastarfeizabadi. On thermal radiation effect in the mhd jeffery–hamel flow of a second grade fluid. *Int J Res Appl Sci Eng Technol*, 2(vii):219–233, 2014.

[13] S Pramanik. Casson fluid flow and heat transfer past an exponentially porous stretching surface in presence of thermal radiation. *Ain Shams Engineering Journal*, 5(1):205–212, 2014.

[14] ATM M Rahman, M S Alamb, and MJ Uddinc. Influence of magnetic field and thermophoresis on transient forced convective heat and mass transfer flow along a porous wedge with variable thermal conductivity and variable prandtl number. *International Journal of Advances in Applied Mathematics and Mechanics*, 3(4):49–64, 2016.

[15] A Rostami, M Akbari, D Ganji, and S Heydari. Investigating jeffery-hamel flow with high magnetic field and nanoparticle by hpm and agm. *Open Engineering*, 4(4):357–370, 2014.

[16] A Salih. Conservation equations of fluid dynamics. 2011.

[17] Lawrence F Shampine, Jacek Kierzenka, and Mark W Reichelt. Solving boundary value problems for ordinary differential equations in matlab with bvp4c. *Tutorial notes*, 2000:1–27, 2000.

[18] M Sheikholeslami, H Mollabasi, and DD Ganji. Analytical investigation of mhd jeffery–hamel nanofluid flow in non-parallel walls. *International Journal of Nanoscience and Nanotechnology*, 11(4):241–248, 2015.